Multifunctional Gadolinium bearing Iron Oxide-Gold Nanoparticles for theranostic application

Vital Cruvinel Ferreira Filho

Instituto Superior Técnico
University of Lisbon
Lisbon, Portugal
vital.filho@tecnico.ulisboa.pt

December 2022

***Abstract* – Superparamagnetic iron oxide nanoparticles (SPIONs) have been progressively studied due to their excellent magnetic behavior, favoring their application in medicine, both in diagnosis and therapy. For example, in the diagnosis and follow up of cancer diseases by magnetic resonance imaging and in their therapy by hyperthermia. Moreover, coating these nanoparticles with an organic material, with long-chain surfactants, or by an inorganic material, such as gold, can improve their stability and make them more versatile.**

The present work aimed to explore a new and original approach in the systematic preparation of multifunctional magnetic nanoparticles, based on SPIONs cores, coated with a polymer, dextran, and gold nanoparticles functionalized with a chelating agent, TDOTA, for the complexation of Gd^{3+} to enhance theranostic applications. In order to optimize the method for obtaining these nanomaterials, three synthesis routes for the SPIONs were designed: the first (method A) by co-precipitation with iron reduction using sodium sulfite ($NaSO_3$); the second (method B) by regular co-precipitation using iron ions (II and III), followed by hydrothermal treatment. A third synthesis method (method C) was also used, although according to this only the naked SPIONs were obtained, without any coating. In this method, co-precipitation with different ratios of iron ions (II and III) was used, compared to method B. Additionally, precipitation step was controlled at pH 9.6.

The nanoparticle samples obtained by the 3 methods and the samples with the subsequent coating were characterized structurally and morphologically by powder X-ray diffraction (PXRD), Mössbauer spectroscopy, transmission electron microscopy (TEM), zeta potential (ζ), dynamic light scattering (DLS), and inductively coupled plasma – mass spectrometry (ICP-MS). Their magnetic behavior was also studied using a magnetometer (SQUID), revealing the presence of superparamagnetic behavior in all of them, essential for further studies.

Viability tests of the samples obtained according to methods A and B were performed on prostate cancer cells (PC3) in order to have insight into their biomedical viability. These preliminary studies revealed that in-vitro studies on PC3 cells can be performed with dilutions of these nanoparticles containing up to 50 µg/mL of iron.

At the end of this work it was concluded that the synthesized nanoparticles provide morphological and magnetic qualities that could be used in *in vitro* and *in vivo* tests for future MRI and magnetic hyperthermia assays in a cell line.

Keywords: SPIONs, Magnetic nanoparticles, Multifunctional nanoplatforms, Gold plating, Gadolinium functionalization, Cancer theranostics, Hyperthermia, Magnetic resonance imaging.

I. INTRODUCTION

Cancer is a major life-threatening disease, and its incidence and mortality are growing rapidly worldwide and are the leading cause of death before the age of 70 in 112 countries. According to estimates, there were 19.3 million new cancer cases and about 10 million deaths in 2020 [1]. Current cancer treatment still relies heavily on surgical intervention, as traditional anti-cancer treatments such as chemotherapy, radiotherapy are not always efficient and often have several drawbacks related to toxicity and lack of specificity [2]. The application of a personalized therapy and the monitoring of its effectiveness usually depend on image-based diagnostics. In this context, there is currently great excitement about the prospects of developing specific theranostics drugs: compounds that simultaneously combine functions with potential for targeted therapy and imaging. Theranostics compounds can be based on molecular or nanosized constructs. Due to their unique physical characteristics and ability to perform at the cellular and molecular level [3], magnetic nanoparticles (MNPs) are an important class of nanostructured materials with potential cancer-theranostic applications, such as hyperthermia treatment, and magnetic resonance imaging (MRI) of tumor cells. In addition, they have been proposed for use as a targeted drug delivery system because, since these magnetic nanoparticles are easily controlled by the application of an external magnetic field, it will allow the release of the anticancer drug at a specified rate and location [4,5].

SPIONs are nanoparticles formed by small iron oxide crystals (commonly magnetite Fe_3O_4 or maghemite $\gamma - Fe_2O_3$), whose core ranges from 10 nm to 100 nm in diameter [6]. Due to the small size these oxides present superparamagnetic properties and consequently SPIONs are considered as a multipurpose class of medicinal agents. Among all their biomedical applications the most frequently explored for cancer therapy are hyperthermia, local chemotherapy and magnetically guided photodynamic and, in the field of diagnosis, the magnetic resonance imaging (MRI). Magnetic hyperthermia therapy consists in using an alternated magnetic field with a given frequency to induce a magnetic signal in the nanoparticles (NPs), which then release energy in the form of heat promoting temperature increase near cancerous tissues. To use this technique as an effective clinical treatment, it is mandatory to produce suitable magnetic nanoparticles that, besides releasing the necessary energy locally, should be non-toxic for the patients. Physiological instability, free radical generation, and inappropriate interface binding may limit the use of naked SPIONs in biomedicine. Therefore, for their use in the biomedical field, it is essential, to coat the NPs, since this may reduce their tendency to aggregate, and improve their colloidal stability and biocompatibility [7]. Additionally, coating allows the conjugation of inorganic components such as silica or gold that are also suitable candidates for the functionalization of the NPs, making them highly desirable for use in biomedical settings. Gold-coated magnetic nanoparticles can be used for so many applications as they are highly versatile whereby the optical and magnetic properties of the particles can be tuned and tailored to the applications by changing their size, gold shell thickness, shape, charge, and surface modification by the attachment of various bioactive molecules such as peptides, antibodies,

aptamers and (radio) metals to further improve diagnosis and treatment efficiency. Nevertheless, depending on the gold shell thickness, charge, and surface modification, the gold coating can dramatically affect the magnetic properties of the final nanoparticles and consequently thus biomedical performance.

This thesis aims to outline a novel and original strategy for the design and evaluation of multifunctional nanoparticles based on SPIONs covered with dextran polymer and gold coated, bearing Gd^{3+} complexes (Figure 1) that can potentially be suitable for diagnosis and therapeutic applications (theranostics). We aim to profit from the optical properties of Au and with the magnetic properties of Fe_3O_4 to obtain nanoplatforms that could potentially be suitable for diagnosis with dual-mode (T1/T2) MRI contrast agents and therapeutic applications (magnetic hyperthermia).

There are several methods and variations to synthesize SPIONs, including hydrothermal synthesis, co-precipitation, microemulsion, and thermal decomposition. In this work, the synthesis of SPIONs by using different approximation methods and their further coating and their subsequent characterization is presented. This characterization included the use of different structural, chemical, and physical methods, such Powder X-Ray Diffraction (PXRD), Transmission Electronic Microscopy (TEM), Dynamic light Scattering (DLS), Zeta Potential, Inductively Coupled Plasma – Mass Spectrometry (ICP-MS), Mössbauer Spectroscopy, magnetization, and magnetic hyperthermia.

Furthermore, the in vivo cellular cytotoxic assays performed in Gastrin Releasing Peptide Receptor (GRPR) overexpressing prostate carcinoma cell lines (PC3) are also presented.

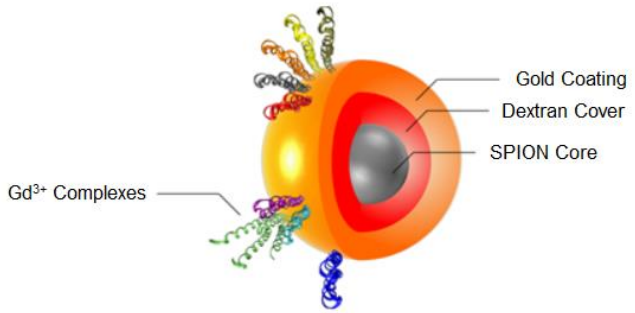

Figure 1: Scheme of the multifunctional nanoplatform designed for this work which consists in a SPION core, covered with dextran polymer, gold coated, and functionalized with complexed Gd^{3+} in TDOTA.

II. EXPERIMENTAL PROCEDURE

A. *Materials*

All chemicals and solvents were of reagent grade and were used without additional purification, unless otherwise stated, and were commercially acquired from Aldrich Chemical. The deionized water was produced from a Millipore system Milli-Q ≥18 MΩcm (with a Millipak membrane filter 0.22µm).

The following materials were used in the preparation of the SPIONs: Iron (III) chloride hexahydrate ($FeCl_3.6H_2O$), iron (II) chloride tetrahydrate ($FeCl_2.4H_2O$), sodium sulfite ($NaSO_3$), ammonium hydroxide (NH_4OH) (25%), hydrochloric acid (HCl, 37%), dextran (Dx) from *Leuconostoc mesenteroides* (average mol wt. 9.000-11.000), amino – dextran (Dx-NH_2), sodium hydroxide in pellets (NaOH), gold (III) chloride acid trihydrate ($HAuCl_4.3H_2O$), sodium borohydride ($NaBH_4$), and gadolinium (III) chloride ($GdCl_3$) .

The polymeric precursors Dx-NH_2 [8] and the ligand 2-[4,7-bis(carboxymethyl)-10-[2 (3sulfanylpropanoylamino)ethyl]-1,4,7,10 tetrazacyclododec1 yl] acetic acid (TDOTA) were previously synthesized and characterized in the Radiopharmaceutical Sciences Group (C^2TN/IST) and kindly provided by Maria Paula Cabral Campello

The PC3 cell line was obtained from ATCC, Manassas, VA, USA.

B. *Synthesis*

The nanoparticles investigated in this work were synthesized by the co-precipitation method but with different approaches for each process.

Co-precipitation is possibly the simplest method for creating nanoparticles of iron oxide. It is possible to employ materials and chemical agents that are harmless and biocompatible, making them suitable for biomedical applications. It is possible to create a fine suspension of NPs with diameters as small as 5 nm by carefully manipulating the reaction conditions. A strong base is added to a solution of, Fe^{2+} and, Fe^{3+} in a molar ratio of 1:2 under an inert or atmospheric environment, resulting in a precipitate Fe_3O_4. Equation 1 shows the co-precipitation reaction for obtaining SPIONs:

$$Fe^{2+}{}_{(aq)} + 2Fe^{3+}{}_{(aq)} + 8OH^{-}{}_{(aq)} \rightarrow Fe_3O_{4(s)} + 4H_2O_{(l)} \quad (1)$$

1) *A Samples (Iron Reduced with Na_2SO_3)*

The synthesis of Naked SPIONs A (A01) was based on the method described by *Matos et al., 2019* [9], consisting of Fe^{3+} reduction with Na_2SO_3 followed by Fe_3O_4 precipitation through titration with NH_4OH. The precursor was separated by centrifugation and lyophilized.

An initial solution was prepared by dissolving 16.67 mmol of $FeCl_3.6H_2O$ in 2.5mL HCl (2M) and 2.5mL deionized water. The second solution was prepared by dissolving 3.33 mmol of Na_2SO_3 in 3 mL of deionized water. Then, solution 1 was carefully added to solution 2 with magnetic stirring at a moderate level at RT and P_{atm}. A solution containing 125 mL of NH_4OH (25 % w/w) was added drop by drop to the resulting solutions of 1 and 2. Due to the precipitation of Fe_3O_4, the color of the solution becomes dark during this phase. The final product was stirred magnetically for 30 minutes, then covered with aluminum foil and capped. Approximately 50 mL of the resulting solution was set aside and stirred for more 24 hours prior to being coated with Dextran. The solution was washed twice with deionized water in a centrifuge under 4000 RPM for 10 minutes and then freeze-dried for 24 hours. Naked SPIONs (A01) were produced as a result of this synthesis.

2) *B Samples (Post hydrothermal treatment)*

For Naked SPIONs B (B01) a method adapted from *Soares et al., 2014* [10] was followed, consisting of a standard co-precipitation process (Equation 1), using Fe^{3+} and Fe^{2+} in a 2:1 mol ratio followed by Fe_3O_4 precipitation using NH_4OH and it was subjected to a post hydrothermal treatment in an effort to control the growth of the nanoparticles size. The precursor was separated by magnetic separation and lyophilized.

to obtain a molar ratio of 2:1 (Fe^{3+}:Fe^{2+}), 5 mmol of $FeCl_3.6H_2O$ and 2.5 mmol of $FeCl_2.4H_2O$ were dissolved in 25 mL of deionized water. Under mechanical stirring, 10 mL of ammonium hydroxide NH_4OH (25%) was quickly added to initiate the reaction. The color change of the mixture from orange to black evidenced the formation of Fe_3O_4. After 5 minutes, the reaction

was stopped by adding 60 mL of deionized water. The total synthesis was performed in nitrogen atmosphere (N_2) in an effort to minimize the oxidation of the synthesized SPIONs. The SPIONs obtained were washed 5 times with deionized water using a strong magnet and then dispersed in water.

a) Hydrothermal treatment

75 mL of SPIONs solution was heated inside the vessel of the equipment to 160 °C and the temperature was kept constant for a reaction time of 16 hours. The container was naturally cooled to room temperature in about 3 hours. The resulting precipitate was washed 4 times in deionized water, to remove the remaining impurities from the SPIONs, and dispersed into deionized water for freeze-drying during 24 hours.

3) C Samples (Controlled environment at pH 9.6)

Naked SPIONs C (C01) was based on the method of Saraiva et al., 2021 [11] which consists of a standard co-precipitation process (Equation 1) but with Fe^{3+} and Fe^{2+} in the proportion of 1:2 mol, respectively. This is an attempt to increase the number of Fe^{2+} ions in solution since the structure that we aim to obtain in larger quantities is magnetite, because it has a better magnetic behavior, and for its formation it is necessary to have a good quantity of Fe^{2+} ions in solution because these oxidize easily to Fe^{3+}. The Fe_3O_4 was precipitated using NH_4OH and the precursor was separated by decantation and lyophilized.

Two solutions of $FeCl_3.6H_2O$ (0.01M) and of $FeCl_2.4H_2O$ (0.02M), were prepared and then mixed. The resultant solution was taken to de-aerate with N_2 for 10 minutes to remove excess oxygen bubbles that could oxidize the iron. After deaeration, NH_4OH (25% w/w) was slowly poured into the solution to promote Fe_3O_4 precipitation. By the time the solution meets the ammonium hydroxide, it is already possible to observe the precipitation by the color change of the solution from yellow to black. The pH of the solution, then, was measured with the help of an equipment and adjusted by ammonium hydroxide until it was 9.6. The solution was then set aside to decant for 24 hours and was non-washed. The excess water was removed, and the precipitate was lyophilized.

4) Dextran Coating

Two different polymeric coating based on dextran were used to cover the naked SPIONs. A01 was covered with dextran (Dx) from *Leuconostoc mesenteroides,* average mol wt. 9.000-11.000 and B01 was covered with Dextran-NH_2 (Dx-NH_2) [8]. The procedure used in both syntheses was based on the method reported by *Matos et al., 2019* [9].

a) Dextran SPIONs (A02)

To the 50 mL (9.1 mg/mL) of Naked SPIONs (A01) solution that was set aside, 6 mL of NaOH (0.5M) was added. In a second solution with 6 mL of NaOH (0.5M), 240 mg of dextran (Dx) was added. Then the suspension of SPIONs was slowly added to the polymer solution under intense magnetic stirring at RT and P_{atm} and left for 24 hours under moderate magnetic stirring, capped, and covered with aluminum foil. The solution was centrifuged the first time to remove its polymer excess. The Dextran SPIONs (A02) was then washed four times with deionized water for 10 minutes at 4000 RPM. The pH after washing was around 8 to 9. The A02 nanoparticles were freeze-dried for 48 hours.

b) Dextran - NH_2 SPIONs (B02)

108,64 mg of Naked SPIONs B01 disperses in 1.4 mL of NaOH (0.5M) was slowly added to the polymer solution of 56mg of Dx-NH_2 diluted in 1.4 mL of NaOH (0.5M), under intense magnetic stirring and left for 24 hours under regular magnetic stirring. The resultant Dx–NH_2 SPIONs (B02) were centrifuged 10 minutes at 4000 RPM, to remove excess polymer from the solution, then washed four times with deionized water and freeze-dried for 48 hours. pH after washing was between 8 to 9.

5) Gold coating

SPIONs gold coated (A03 and B03) were made based on a mixture of methods from *Caro et al., 2021* [12] and *Elbialy et al., 2014* [13].

6) Gadolinium Functionalization

The Gadolinium functionalization was made *via* a T-DOTA chelating agent, based on a previous work from the Radiopharmaceutical group of C2TN [14].

Two solutions were made, one with 140mg of A03 and 1mL of ethanol and the other with 140 mg of B03 and 1 mL of ethanol. These solutions were sonicated for 5 minutes. Meanwhile, another two solutions made of 500 µL of ethanol with 140 mg of the chelator agent T-DOTA were placed under a magnetic stirring. After sonication, the solutions of SPIONs were placed in a solution of T-DOTA and left capped and covered with aluminum foil for 10 hours.

After this process, two solutions consisting of 40 mg (0.108 mmol) of $GdCl_3$ and 5 mL of deionized water each were prepared. One solution was added to A03 with T-DOTA and the other to B03 with T-DOTA. The solutions were left on the magnetic stirring, capped and covered with aluminum foil for 16 hours. The reaction started at pH close to 6 and ended at pH between 4 and 5. Following this process, the solutions were washed twice with deionized water at 6000RPM for 10 minutes and freeze-dried for 48 hours to obtain the Dextran SPIONs@Au – Gd^{3+} (A04) and Dextran NH2 SPIONs@Au – Gd^{3+} (B04).

All samples made in this work are represented in Table 1 below with their identification and name.

Table 1: Labels for each kind of sample

Samples	Description	Labels
Naked SPIONs	Iron Reduced with Na_2SO_3	A01
Naked SPIONs	Post hydrothermal treatment	B01
Naked SPIONs	Controlled final pH 9.6	C01
Dextran SPIONs (Dx-SPIONs)	SPIONs covered with Dx	A02
Dextran – NH_2 SPIONs (Dx-NH2 SPIONs)	SPIONs covered with Dx – NH_2	B02
Dextran SPIONs@Au	SPIONs covered with Dx, and gold coated	A03
Dextran – NH_2 SPIONs@Au	SPIONs covered with Dx – NH_2 and gold coated	B03
Dextran SPIONs@Au – Gd^{3+}	SPIONs covered with Dx, gold coated functionalized with Gd^{3+} complexed TDOTA	A04
Dextran – NH_2 SPIONs@Au – Gd^{3+}	SPIONs covered with Dx – NH_2, gold coated functionalized with Gd^{3+} complexed TDOTA	B04

C. SPIONs Characterizations

SPIONs were characterized by dynamic light scattering and zeta potential (DLS), transmission electron microscopy (TEM), Powder X-ray diffraction (PXRD), Mössbauer spectroscopy, SQUID magnetometry, and magnetic hyperthermia. Iron, Gold and Gadolinium content was determined by Content by Inductively Coupled Plasma Mass Spectroscopy (ICP-MS).

1) Powder X-Ray Diffraction

Measurements were performed in the D2 PHASER diffractometer-Bruker with a Cu source and a wavelength of λ = 1.54 Å. The spectrum was collected at room temperature between angles (2θ) of 10º and 80º with a step size of 0.01º, time per step of 10.5 s, 3 RPM, and PSD opening of 3º. For sample preparation, a small volume of sample powder was placed on a standard support used for this technique, and ethanol was used to settle the powder on it.

2) Mössbauer Spectroscopy

Mössbauer spectra were collected at room temperature and 4 K in transmission mode using a conventional Wissel constant-acceleration spectrometer and a 25 mCi ^{57}Co source in a Rh matrix. The velocity scale was calibrated using α-Fe foil. Isomer shifts, IS, are given relative to this standard at room temperature. The absorbers were obtained by packing the powdered samples into perspex holders. Absorber thicknesses were calculated on the basis of the corresponding electronic mass-absorption coefficients for the 14.4 keV radiation, according to Long *et al*. 1983 [15]. Low-temperature measurements were performed with the sample immersed in liquid He in a *Janis bath cryostat, model SVT-400*. The spectra were fitted to Lorentzian lines using a non-linear least-squares method. Relative areas and line widths of both peaks in a quadrupole doublet and of peak pairs 1-6, 2-5 and 3-4 in a magnetic sextet were constrained to remain equal during the refinement procedure. Distributions of magnetic splittings were fitted according to the histogram method [16].

3) Transmission Electronic Miscroscopy (TEM)

The transmission electron microscopy (TEM) images were obtained on a FEI Tecnai G2 Spirit BioTWIN transmission electron microscope. The samples for the TEM analyses were prepared by dipping a 300-mesh carbon-coated copper grid into a solution containing SPIONs previously sonicated. The carbon grid dried for 5 min. Software Image-J was used to process the obtained images in order to determine the average size of the SPIONs.

4) Inductively Coupled Plasma Mass Spectrometry (ICP-MS)

ICP-MS measurements were performed on *Thermo X Series* equipment at the University of Aveiro's LCA (Laboratório Central de Análises). Four samples were sent to be analyzed for the concentrations of Fe, Au, and Gd in each one. Samples were dry weighed before being sent to Aveiro.

5) DLS and Zeta Potential

DLS measurements were performed with a Malvern Zetasizer Nano ZS (Malvern Instruments Ltd., Worcestershire, UK) equipped with a 633 nm He-Ne laser and operating at an angle of 173º. The software used to collect and analyze the data was the Dispersion Technology Software (DTS) version 5.10 from Malvern. 600 L of each sample was measured in low volume semi-micro disposable sizing cuvettes (Fisher Scientific, USA) with a path length of 10 mm. Triplicate measurements were made at a position of 4.65 mm from the cuvette wall with an automatic attenuator. For each sample, 15 runs of 10 s were performed. The hydrodynamic size and the polydispersity index (PDI) were obtained from the autocorrelation function using the “general purpose mode” for all nanoparticle samples. The default filter factor of 50% and the default lower threshold of 0.05 and upper threshold of 0.01 were used. Zeta potential measurements were performed in triplicates using water as a dispersant and the Huckel model. For each sample, 20 runs were performed in auto analysis mode.

6) Magnetometry (SQUID)

Static magnetic measurements were obtained using the *SQUID* (Superconducting Quantum Interference Device) magnetometer system. The SQUID magnetometer is the most sensitive, and perhaps the most widely used technique to measure the magnetic properties of a material. In this work a S700X SQUID Magnetometer from the company Cryogenic Ltd. was used.

a) Magnetization vs. Field

M(H) curves were taken at a temperature of 300 K and 10 K. These measurements were made to assess the saturation of magnetization (M_s). These measurements will allow us to analyze the variations of these properties for each SPIONs samples obtained from different synthesis processes and their further coatings and functionalization.

b) ZFC/FC

The samples were cooled from 300 K to 10 K in a zero magnetic field, then a static magnetic field of 2.5 mT for the Naked SPIONs and Dextran SPIONs and 50 mT for the gold coated and gadolinium functionalized ones was applied. The ZFC curve was measured while the samples were heating. The samples were once more cooled to 10 K while keeping the same field (FC procedure) after the last point was measured, and data was then measured for rising temperatures.

7) Magnetic Hyperthermia

Magnetic hyperthermia measurements were obtained using a DM100 series from *Nb Nanoscale Biomagnetics* apparatus. This apparatus allows measurements at different magnetic field intensities up to 300 Gauss with a frequency up to 418.5 kHz.

It was evaluated the heating ability of naked SPIONs (B01), coated with dextran (B02) and gold coated (B03) at a concentration of 1 mg/mL. Measurements were performed during 10 minutes by keeping magnetic field intensity of 300 Gauss and constant frequency of 388.15 kHz.

8) Cytotoxicity Assay

For the evaluation of the cytotoxic activity of the SPIONs a human prostate cancer cell line PC3 (ATCC, CRL-1435) was selected. The cell culture was prepared using RPMI-1640 (Roswell Park Memorial Institute Medium) supplemented with 10% fetal bovine serum (FBS) and 1% antibiotics. The cells were suspended in the medium, placed in culture flasks and incubated at 37ºC in the presence of CO_2 (5%). Upon confluence, the cells were removed by treatment with trypsin/EDTA solution, suspended with a complete medium and further diluted for cell counting or sub-culturing. The 3-(4,5-dimethylthiazol-2-yl)-2,5-diphenyl-2H-tetrazolium bromide (MTT) assay was used to evaluate the cellular viability. This assay is based on the reduction of the soluble yellow tetrazolium salt to insoluble purple formazan crystals by a succinate dehydrogenase enzyme, which is present in the mitochondria of metabolically active cells. For the assays, the cells were seeded into 96-cell plates at a density of 2 x 10^4 cells/200 µL. After a period of 24 h for adherence, the cells were treated with 200 µL of different concentrations of A01, A04, B01

and B04 SPIONs in the range of 10 to 500 µg of Fe/mL and were incubated at 37 ºC for 24h in the presence of CO_2 (5%). After the incubation, the medium was aspirated and 200 µL MTT solution in PBS (0.5 mg/mL) was added to the cells. The latter were further incubated for another 3h under the same conditions. Finally, the formazan crystals were dissolved in 200 µL DMSO and the absorbance was measured with a microplate reader at 570 nm (Power Wave Xs, Bio-Tek, Winooski, VT, USA). The absorbance of the untreated cells was used as the control.

III. Results and Discussion

A. Structural characterization

Powder X-ray diffraction measurements reveal structural information, phase, and approximate size of the crystalline core of the SPIONs. In the diffractograms for all A, B, and C samples, the diffraction pattern showed peaks at 2θ of approximately 18.50°, 30.31°, 35.72°, 43.40°, 53.80°, 57.35°, and 62.94°, consistent with nano-sized crystallites, allowing the identification of the main peaks of a spinel phase. The unit-cell parameters were estimated from the PowderCell program. From these parameters it was possible to infer that both magnetite, Fe_3O_4 (JCPDS file 19–629), and maghemite, γ – Fe_2O_3 (JCPDS file 39–1346), are present. Magnetite with ideal stoichiometry and maghemite. These two phases have the same crystalline planes for the main peaks but with slightly different intensity. This hinders the distinction between magnetite and maghemite with this technique. However, these two compounds can be distinguished by using another characterization technique, the Mössbauer spectroscopy, which allows to identify Fe-containing phases and their oxidation state, Fe^{2+} and Fe^{3+} (see below in this section). Figure 2a, b and c show the comparison between the diffractograms of naked SPIONs (A01, B01 and C01).

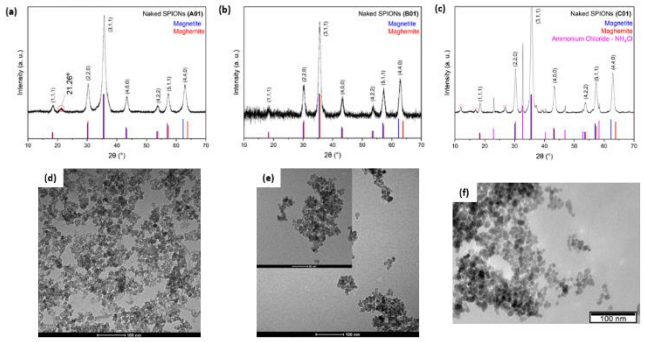

Figure 2: Powder X-Ray Diffractogram of samples A01 (a), B01 (b) and C01 (c). TEM images of samples A01 (d), B01 (e) and C01 (f).

For A01 it is possible to observe a peak at 21.26º (Circulated in red) that is neither part of the magnetite nor of the maghemite. Through literature searches and analysis with the software DIFRACC.EVA it is possible to attest that this peak refers to a slightly presence of goethite that is an Iron (III) oxide - Hydroxide (α - FeO(OH)) [17].

Naked SPIONs C01 sample show the appearance of an ammonium chloride (NH_4Cl) salt phase (JCPDS file 73-1491) [18]. The presence of this salt comes probably from the non-washing of SPIONs C in the synthesis step. In addition, it is possible to observe non-main peaks (circled in red) which suggest the presence of maghemite. This fact may reveal that this sample has a higher amount of maghemite when compared to the naked SPIONS A01 and B01.

The X-ray diffraction measurements for A04 and B04 (Figure 3) showed peaks at 2θ for the gold phase at, approximately, 38.15º, 44.32º, 64.56º, 77.53º. Comparing with the JCPDS card for gold (Au^0) (JCPDS 04-0784), it is observed that the samples have peaks corresponding to this FCC structure.

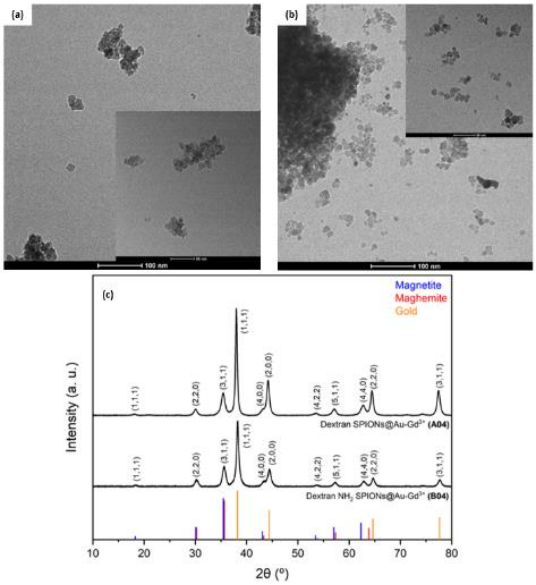

Figure 3: TEM images of samples A04 (a) and B04 (b). Powder X-Ray Diffractogram of samples A04 and B04 (c).

Even though the samples have more percentage of iron than gold, the peaks for gold are more intense due to the high absorption of radiation by the gold nanoparticles [19], causing the iron oxide peaks to be somewhat faded.

By this technique it is not possible to confirm if gadolinium is present in samples A04 and B04, because it is in ionic form (Gd^{3+}) complexed by the chelator agent T-DOTA. In order to fully identify all the metals present in these samples ICP-MS measurements were undertaken for samples A01, A04, B01 and B04. The results shown that gadolinium is present in samples A04 and B04 in amounts of 0.410 and 0.173% of these samples, respectively. In addition, with the amount of gold and iron also obtained, it was possible to evaluate the proportion between these two elements in mol obtained after synthesis. These results suggest that samples A03 and B03 were coated with gold in a mol ratio of approximately 4Fe:1Au.

Using the 3 main peaks from the PXRD data of the samples, the crystallite size (D_{XRD}) of the iron core of each sample was evaluated by using Debye Scherrer's equation ((2) [20]:

$$D_{XRD} = \frac{K\lambda}{\beta Cos(\theta)} \qquad (2)$$

where K is the Scherrer constant equal to 0.9 for spherical particles, λ is the X-ray wavelength of λ=1.54Å, β is the full width at half maximum (FWHM) in radian, and θ is the Bragg angle of the peak position in radians. The crystallite sizes, estimated by (, for the different samples ranged between 7.78 and 10.55 nm and are arranged in Table 2

Table 2: Measurements of sizes obtained by PXRD, TEM, SQUID, DLS and zeta potential of all samples.

Sample	Crystallite Size D_{XRD} (nm)	Particle size D_{TEM} (nm)	Magnetic Diameter D_{MAG} (nm)	Hydrodynamic Size D_H (nm) (PDI)	Zeta Potential (mV)
A01	9.04	10.02 ± 2.10	10.51	108.95 (0.482)	40.3 ± 8.10
A02	7.79	6.60 ± 1.82	11.00	352.40 (0.373)	-6.21 ± 7.64
A03	9.81	10.91 ± 2.71	11.68	223.64 (0.536)	-1.91 ± 6.04
A04	9.40	11.34 ± 2.75	12.28	133.80 (0.490)	35.35 ± 8.50
B01	9.84	9.85 ± 1.97	9.55	84.02 (0.357)	-13.13 ± 6.15
B02	9.60	9.76 ± 2.12	11.72	118.80 (0.484)	47.83 ± 8.14
B03	10.55	10.00 ± 2.27	11.85	87.80 (0.731)	47.01 ± 7.03
B04	9.76	11.02 ± 2.21	13.13	44.70 (0.511)	44.80 ± 9.11
C01	9.98	8.30 ± 1.73	9.84	19.00 (0.537)	43.80 ± 9.73

As confirmed by the Mössbauer spectroscopy technique performed for samples A01, A02, A03, B01, and B03, the magnetite present in those samples is partially oxidized. There is no reason to believe that all the spinel grains have exactly the same oxidation degree. Most probably magnetite grains with different oxidation degrees up to the maghemite limit where all the Fe cations are in the 3+ oxidation state, are present in the studied samples leading to a mixture of spinel grains with different unit-cell parameters. This further broadens the PXRD peaks, in addition to the small grain size effect. Mössbauer spectroscopy technique performed show that these samples have on average 13% magnetite

The transmission electron microscopy (TEM) technique was used to evaluate the size, shape, and size dispersion (σ) of the produced SPIONs. The average nanoparticle size (D_{TEM}) was calculated from the TEM images shown in this section, using the Image-J program. From the obtained values, the histograms presented were constructed using sample sizes (N) of 100 and 200.

A01 nanoparticles have a D_{TEM} of 10.02 ± 2.10 nm, a mixture of spherical and cubic shapes and some undefined shapes and a σ of 20,94%, while B01 and C01 have nanoparticles with a D_{TEM} of 9.85 ± 1.97 nm, with predominantly spherical morphology and a σ of 19,98% and a D_{TEM} of 8.30 ± 1.73 nm, well-defined spherical shape with a few variations and a size dispersion of 20.8%, respectively. All results for D_{TEM} are shown in Table 2.

When particles interact, two forces must be considered, van der Waals and electrostatic repulsion. Based on these interactions, the zeta potential (ζ) is calculated as the ratio between the speed at which the particles move in suspension and the electric field applied at the time of measurement. This technique measures the electrostatic potential at the boundary of the compact layer and the diffuse layer of the colloidal particles, demonstrating the degree of stability of the suspension [21]. In absolute value, the higher the zeta potential, the greater the repulsion between the particles, so they tend to become dispersed. If the zeta potential is close to 0 mV they tend to agglomerate [22].

As reported in the literature, it is a general rule that good particle stability has zeta potential values above 30mV or below -30mV. Values around 5mV indicate a fast aggregation of the particles [23].

Zeta values determined for all samples are presented in **Error! Reference source not found.**. Naked samples A01 and C 01 obtained ζ of 40.3 ± 8.1 and 43.80 ± 9.7 mV, respectively. This indicates good stability and dispersion of the particles as also confirmed from the TEM analyses. For C01 the ζ value is due to the fact that sample was not washed, causing a large amount of NH_4^+ and Cl^- ions from the synthesis to be adsorbed on the surface of the SPIONs. As shown by PXRD, C01 has peaks related to ammonium chloride NH_4Cl. The high positive value of the zeta potential of A01 can also be attributed to the adsorption of Na^+ and NH_4^+ ions on the surface of the SPIONs aggregates due to an inefficient washing. For sample B01, a zeta potential of -13.13 ± 6.1 mV was determined, which reveals a low stability and less dispersion. This may be due to a more efficient washing process by magnetic separation in removing adsorbed positive ions from the SPIONs, possibly leaving only adsorbed Cl^- ions, and consequently making this potential to be negative.

The addition of Dx and Dx-NH2 in A02 and B02, respectively, implies a change of the ζ. Negative OH^- groups from the dextran and sodium hydroxide OH^- groups that replaces the other adsorbed ions at the SPIONs surface, cause the ζ in A01 to decrease to a value of -6.21 ± 7.6 mV, indicating instability and lower dispersion of the suspension. On the contrary, for B02, where Dx - NH2 was used, which has a much more positive character due to the amino group present in it, the zeta potential increased and became positive (47.83 ± 8.1 mV), indicating good stability and dispersion. The addition of the gold layer seems to have no effect on the ζ values.

The functionalization with TDOTA complexed Gd^{3+} increased the zeta potential from A03 to A04 (35.35 ± 8.5 mV), which may indicate a stabilization of the nanoparticles at lower pH [24]. The values of zeta potential for B04 (44.80 ± 9.1 mV) are in agreement with the TEM analysis of this sample (Figure 3b), showing good dispersion of the nanoparticles.

The DLS technique correlates the Brownian motion of the particles in a colloidal suspension with the hydrodynamic size (D_H) of the analyzed material. Therefore, to obtain the size it is necessary to analyze the motion of these particles over a certain time. Particles with smaller hydrodynamic sizes diffuse rapidly due to the rapid Brownian motion in solution. However, when the hydrodynamic sizes are larger, the movements are slower, leading to a decrease in Brownian motion [25].

The difference in the size determination of nanoparticles by PXRD (D_{XRD}) and TEM (D_{TEM}), and the mean hydrodynamic size obtained by DLS (D_H), is due to the hydrodynamic radius, a hydration layer related to the electrical double layer of the nanoparticles. The presence of dextran in A02 can be attested due to the large increase in D_H from A01 (108.95 nm) to A02 (352.40 nm). As A02 is composed of small clusters this hydrodynamic size may refer to the whole cluster and not just to a single nanoparticle as shown in Figure 4. In addition, since SPIONs are magnetic, they were attracted by the electrode of the cuvette during the tests, which may have provided inaccurate measurements using this technique.

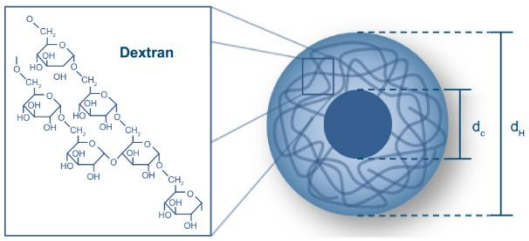

Figure 4: Diameter of magnetic core (d_c) is surrounded by a magnetically neutral coating (Dextran) (with hydrodynamic diameter d_H). Adapted from [95].

The decrease of D_H when samples are coated with gold nanoparticles (A03 and B03) is due to a compression of the gold against the D_H direction. For nanoparticles functionalized with TDOTA complexed Gd^{3+} (A04 and B04), the $-NH_2$ and $-(OH_2)^+$ groups from TDOTA complex the gadolinium inside and outside making a shell around the nanoparticles or nanoparticles aggregates, also reducing its D_H. Table 2 shows a comparison of the diameters obtained by PXRD, TEM and DLS analyses, as well as the values obtained for the zeta potential of each sample.

B. Magnetic Characterizations

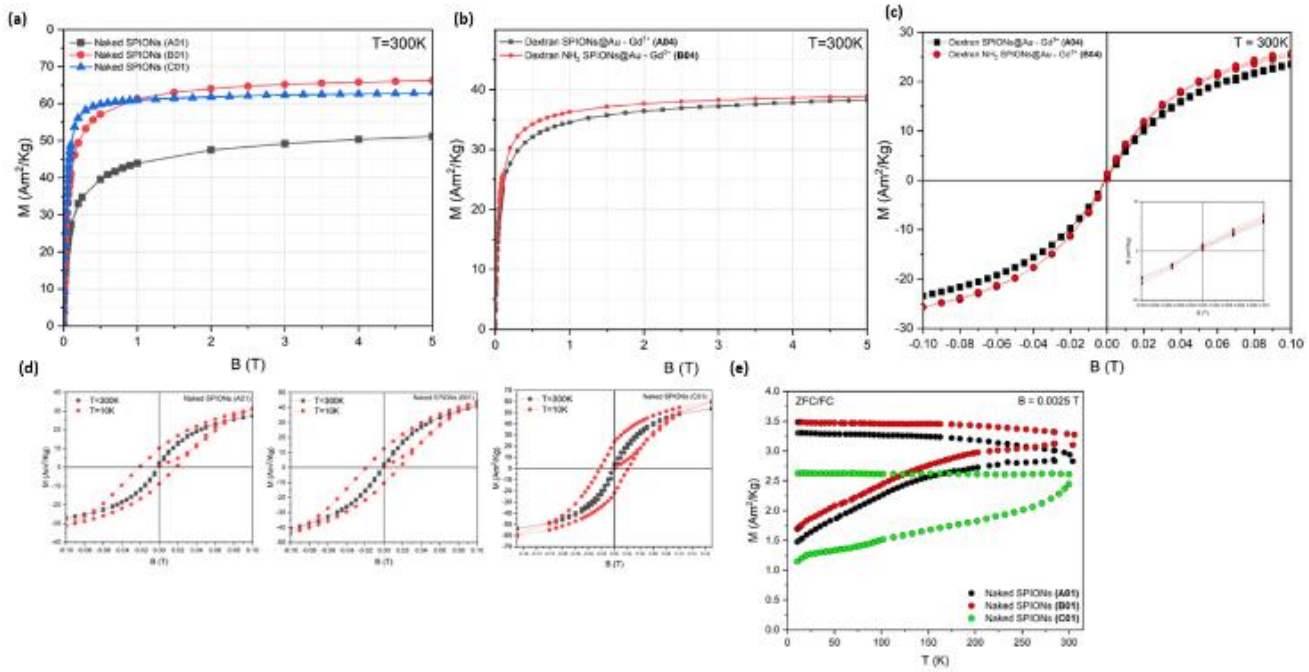

Figure 5: Field dependence of the magnetization for A01, B01, C01 (a). Field dependence of the magnetization for A04 and B04 samples (b) and hysteresis curves showing the superparamagnetic behavior of A04 and B04 at 300K (c). Hysteresis curves showing superparamagnetic behavior at 300K and ferromagnetic behavior at 10K for samples A01, B01, and C01 (d). ZFC/FC curves for Naked SPIONs (A01, B01, and C01) under a magnetic field of 2.5 mT (e).

The magnetic properties of all the nanoparticles samples were performed by means of static (DC) magnetization measuring the hysteresis loops and the thermal dependence of the magnetization after field-cooling (FC) and zero-field-cooling (ZFC). In general, the field dependence of the magnetization curves taken at room temperature, 300 K, showed no hysteresis, with coercivity (Hc) approximately 0, which is indicative of the superparamagnetic behavior required. Moreover, upon removal of the applied magnetic field, the SPIONs retain no residual magnetism at room temperature, which is a good advantage for their use in theranostic, since they do not have tendency to agglomerate, thus enabling the uptake by the tumor cells. The saturation magnetization (M_s) values varied between 51,00 and 66.60 Am^2/Kg for the naked samples (A01, B01, and C01), which are in accordance with other works that synthesized SPIONs through co-precipitation method [26–28]. B01 achieved the highest M_s value of 66 Am^2/Kg, validating the synthesis method B as the one that provided SPIONs with the best magnetic performance so far. This fact can be due to a slightly larger amount of magnetite in B01 has when compared to A01, which also increase its saturation magnetization value. At lower temperatures, i.e., 10 K, the nanoparticles present a higher value of saturation magnetization, and it is necessary to apply a coercive field to reach a magnetization of zero, meaning that at this temperature the nanoparticles exhibit hysteresis and behave as ferromagnets. Figure 5a shows the M(B) curves obtained for A01, B01 and C01 at 300 K

As the SPION cores gradually become more covered, the M_s values tend to decrease, as it happens to samples A04 and B04 (Figure 5b). For sample B04 this decrease reaches approximately 41% which suggest that from B03 to B04 there has been no change in the behavior of the M(B) curve. The M_s value of A04 decreased by 24.9% relative to its naked version. However, although this decrease is detected, they remain superparamagnetic at 300 K (Figure 5c) and present good values of saturation magnetization. This M_s reduction is very low when compared to other values in the literature. In a study by *Stein et al., 2020* [29] SPIONs after gold coating lost 40% of their M_s while in a study by *Elbialy et al., 2014* [13], they lost 32.8%. Therefore, the small reduction that was obtained here in M_s after the coating and functionalization process may be a breakthrough in this research. Overall, these magnetic results ensure that the use of such nanoparticles in biomedical is feasible and can be tested in further in vitro and in vivo assays.

Figure 5e shows the temperature dependence of the ZFC/FC magnetization curves of Naked SPIONs (A01, B01, and C01) measured by SQUID under an applied filed of 2.5 mT. The blocking temperature (T_b) was determined as the maximum value of ZFC curve. Larger nanoparticles require a higher temperature for the thermal energy to exceed the energy barrier, and thus be unlocked, and behave as superparamagnets. At this point there is a guarantee that all nanoparticles in the system are unblocked [30]. Samples A01, B01 and, C01 exhibit a T_b of 283.7, 284.7, and 299.9 K, respectively, which indicates that at RT they have superparamagnetic behavior, confirmed by the absence, at 300 K of coercivity and magnetic remanence, as showed on Figure 5d. In the **Error! Reference source not found.** below T_b values obtained through the ZFC/FC curves for each sample are presented.

Knowing that all the samples exhibit superparamagnetic behavior at RT, it is possible to determine the mean magnetic diameter (D_{MAG}) of the nanoparticles taking into account the M(B) curve obtained at 300 K through the equation below (3) [50]:

$$D_{MAG} = \left(\frac{18 K_b T \left(\frac{dM}{dB} \right)_{(B \to 0)}}{\pi \rho {M_s}^2} \right)^{\frac{1}{3}} \quad (3)$$

where K_b is the Boltzmann constant which is equal to 1.381 x 10^{-23} m^2Kg/s^2K, T is the temperature in Kelvin, $\left(\frac{dM}{dB}\right)_{(B \to 0)}$ is the derivative of first order of the curve M(B) at the point B = 0, M_s is the saturation magnetization, and ρ is the mass density of the iron oxide structure. Although it is known by Mössbauer spectroscopy that the samples contain between 11 to 17% in magnetite, in order

to $$SAR = \frac{C_S m_{Fe} + C_w m_w}{m_{Fe}} \left(\frac{dT}{dt}\right)_{(Max)} \quad (4)$$

simplify these calculations, it was assumed for that all samples have 100% in maghemite, which gives ρ = 4900 Kg/m^3. These calculations are presented in Table 2. By comparing these results with the ones already determined by PXRD and TEM characterization, one can verify a good agreement between all of them.

Table 3: Blocking temperature obtained by the highest value of the ZFC curve for each sample.

Samples	Blocking Temperature - $T_b(K)$
A01	283.68
A02	204.15
A03	87.38
A04	92.10
B01	284.69
B02	102.24
B03	92.27
B04	-
C01	299.92

C. *Magnetic Hyperthermia*

Due to several constraints, magnetic hyperthermia tests were only possible for samples B01, B02, and B03. This study showed that the highest temperature variation [ΔT (ºC)] as a function of time (s) occurred for the sample B01, which reached a variation of 8 °C. Coated samples B02 and B03 have shown practically the same variation, 3.7 ºC for B02 and 3.5 ºC for B03 (Figure 6). B01 sample reaches a temperature higher than 40 °C in approximately 200 s inside a human body in these conditions, whereas B02 and B03 achieves the same temperature only after approximately 500 s. This difference could be attributed to the organic covering of Dx – NH_2 that behave as an insulating shell around the SPION's surface [31].

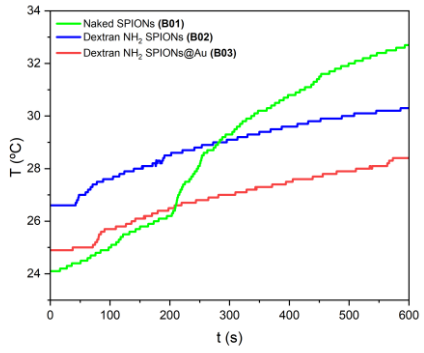

Figure 6: Hyperthermia curves of temperature (ºC) vs. time (s) for B samples.

The parameter known as Specific Absorption Rate (SAR) is used to characterize the heating efficiency of a magnetic material by measuring its energy absorption when exposed to an AC magnetic field. This value is calculated by using the (4) and is defined as the amount of power absorbed by the sample per mass unit (W/g):

Where $\left(\frac{dT}{dt}\right)_{(Max)}$ is the maximum gradient of the temperature curve of the SPIONs in water submitted to the hyperthermia test, C_S is the specific heat of the nanoparticles, C_W is the specific heat of the liquid, m_w is the water mass, and m_{Fe} is the iron mass in the sample. Figure 7 shows the SAR values calculated for B01, B02, and B03.

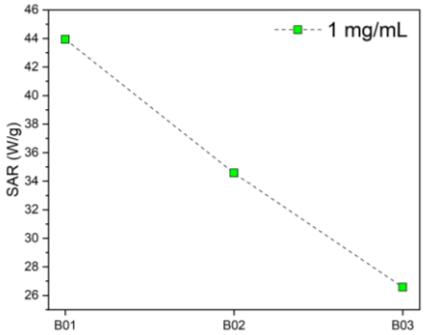

Figure 7: SAR values obtained for B01, B01, and B03.

B samples are promising option for inducing apoptosis in cancer cells at temperatures between 40 and 45 degrees Celsius [32,33]. In addition, the SAR values for B01, B02, and B03 correspond to those reported in the literature [34].

Table 4 shows the values of ΔT (ºC) and SAR through magnetic hyperthermia for B samples.

Table 4: Values of temperature variation (ºC) and SAR (W/g) obtained for B01, B02, and B03.

Sample	ΔT (ºC)	SAR (W/g)
B01	8.7	43.94
B02	3.7	34.57
B03	3.5	26.57

D. *Cytotoxicity Assay*

Although at a preliminary stage, it was still possible in this work to perform cytotoxicity tests in samples A04 and B04. The cytotoxicity of SPIONs has been attributed to both structural factors related to their size, shape, charge as well as their coatings. Therefore, the cytotoxic effect of SPIONs A04 and B04 was studied using the PC3 cells (prostate cancer) in order to obtain information regarding the selection of the most suitable concentrations to use in future studies on the evaluation of these platforms as theranostic agents. The MTT assay, a metabolic assay considered the "gold standard" for cytotoxicity, was selected for the evaluation of the cell viability of these SPIONs.

The results obtained by the MTT assay on the PC3 cells treated for 24h with serial dilutions of SPIONs A04 and B04 (10 to 50 µg Fe/mL) and their respective precursors A01 and B01 are presented in Figure 8. Dilutions in concentration of 100, 200, and 500 µg Fe/mL were removed because they presented a stronger coloration, which interfered with the spectrophotometric measurement. These results show that for concentrations up to 50 µg Fe/mL it is feasible to proceed with tests in PC3 cells, with

the worst-case scenario killing approximately 25% of cells at 25 and 50 µg Fe/mL for sample B04.

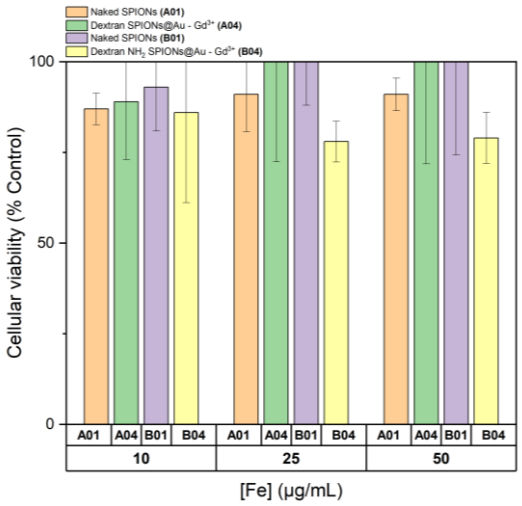

Figure 8: Graphical diagram showing the cellular viability for A01, A04, B01 and B04 samples at different concentrations of Iron.

IV. CONCLUSIONS

The work developed in this thesis had as main objective the synthesis of iron oxide nanoparticles able to be used as a nanoplatform for drug delivery for therapy and imaging. The advantage of such nanosystems is the combination of diagnostics and therapy allowing the possibility to acquire real-time information about the delivery and eventually the effects of therapeutic agents when administered to patients.

These nanoparticles were produced by the chemical precipitation, which provided SPIONs with diameters smaller than 11nm and with magnetizations greater than 50 Am2/Kg. Three different approaches were elaborated. In the first one (A samples) the reduction of Fe was used to obtain the amount of iron ions necessary for precipitation, in the second method (B samples) a hydrothermal post treatment was used and in the third one (C samples) a fine monitoring of the pH to reach 9.5 was made during the precipitation phase of Fe3O4. Method B provided a smaller size dispersion of the nanoparticles, with 19% and samples with the best saturation magnetization of 66 Am^2/Kg while method C showed to be more efficient to obtain samples with smaller particle size of 8.3 ± 1.73 nm through TEM with spherical shape. With method A the shape of the nanoparticles varied greatly, and they also have a goethite phase, which although in low percentage is considered a non-desirable phase for further biomedical applications.

Since iron oxides nanoparticles have a natural tendency to aggregate, surface modification and stabilization of SPIONs A and B was performed by adding Dx and Dx-NH2, respectively. The SPIONs were further covered with a gold shell with the goal to obtain a uniform and continuous coating with a thickness that does not lead to substantial loss of the magnetic performance of the nanoparticles and functionalized with TDOTA complexed gadolinium (III). All the prepared samples were characterized in terms of size, phases, morphology, and stability by a combination of techniques such as, DLS, PXRD, TEM, Zeta Potential, and Mössbauer spectroscopy. The content of metals Fe, Au and Gd have been determined by ICP-MS. A detailed magnetic study by static magnetization to assess their magnetic performance, namely in terms of superparamagnetic (single domain) and blocking behavior was also performed.

ICP-MS analyses reveal that Gadolinium and Gold are present in samples A04 and B04. TEM images show that the final product B04 has a good dispersion of the nanoparticles in the medium, being crucial for theranostic applications.

Magnetization studies have shown that SPIONs core of these samples keep their superparamagnetic behavior assuring the maintenance of the magnetic properties in A04 and B04. Particle size determined by PXRD, TEM and SQUID is about 10.19 nm which is a considerable good size for *in vivo* applications, and it is consistent with other reported studies [87-90].

Analysis by Mössbauer spectroscopy revealed that SPIONs are mainly composed by maghemite with approximate 13% of magnetite, which improve the magnetic character of the samples

Regarding the magnetic hyperthermia tests, due to several constraints it was not possible to perform those measurements for all samples. However, preliminary tests on samples B01, B02 and B03 have shown that sample B01 present a quite significant temperature variation, of 8.7 ºC, and may be efficient to generate the apoptosis of cancer cells that occurs between 40-45ºC [39, 40].

Cytotoxicity assay *in vitro* allowed us to know that concentrations of these samples up to 50 ug Fe/mL do not generate significant damage to PC3 cells, so at these concentrations it is possible to continue with future MRI and Magnetic Hyperthermia tests *in vitro* and later *in vivo*.

The strategy to undertake a systematic study of preparation of SPIONs has proved to be innovative and the results found encouraging providing a clear indication on the potential application of these SPIONs-nanoplatforms as bimodal probes in cancer diagnosis.

V. FUTURE WORK

Despite the large volume of work done in this thesis there are some loose ends concerning different characterization studies, namely:

- The magnetic hyperthermia measurements of all the samples under different conditions of sample concentrations, and operational parameters, such frequency and alternate magnetic field.
- The DLS and zeta potential analysis at different pH values in order to obtain information concerning the stability of such nanoparticles in the physiologic medium (human body). These results could be advantageous to understand and improve further surface modifications of SPIONs.

After all the characterization studies and once cell viability assays are concluded the decision to proceed to *in vitro* and *in vivo* tests on PC3 cells, should be done in order to perform MRI and magnetic hyperthermia assays in those cells.

References

[1] H.-L. Rao *et al.*, “Increased Intratumoral Neutrophil in Colorectal Carcinomas Correlates Closely with Malignant Phenotype and Predicts Patients’ Adverse Prognosis,” *PLoS ONE*, vol. 7, no. 1, p. e30806, Jan. 2012, doi: 10.1371/journal.pone.0030806.
[2] Z. Defu, Y. Ting, Y. Jian, F. Shuang, and Z. Shubiao, “Targeting strategies for superparamagnetic iron oxide nanoparticles in cancer therapy,” *Acta Materialia Inc*, vol. 102, pp. 13–34, 2020, doi: 10.1016/j.actbio.2019.11.027.
[3] C. Sun, J. S. H. Lee, and M. Zhang, “Magnetic nanoparticles in MR imaging and drug delivery,” *Advanced Drug Delivery Reviews*, vol. 60, no. 11, pp. 1252–1265, Aug. 2008, doi: 10.1016/j.addr.2008.03.018.
[4] J. Chomoucka, J. Drbohlavova, D. Huska, V. Adam, R. Kizek, and J. Hubalek, “Magnetic nanoparticles and targeted drug delivering,” *Pharmacological Research*, vol. 62, no. 2, pp. 144–149, Aug. 2010, doi: 10.1016/j.phrs.2010.01.014.
[5] M. K. Lima-Tenório, E. A. Gómez Pineda, N. M. Ahmad, H. Fessi, and A. Elaissari, “Magnetic nanoparticles: In vivo cancer diagnosis and therapy,”

International Journal of Pharmaceutics, vol. 493, no. 1–2, pp. 313–327, Sep. 2015, doi: 10.1016/j.ijpharm.2015.07.059.
[6] S. Laurent *et al.*, "Magnetic Iron Oxide Nanoparticles: Synthesis, Stabilization, Vectorization, Physicochemical Characterizations, and Biological Applications," *Chem. Rev.*, vol. 108, no. 6, pp. 2064–2110, Jun. 2008, doi: 10.1021/cr068445e.
[7] M. R. Faria, M. M. Cruz, M. C. Gonçalves, A. Carvalho, G. Feio, and M. B. F. Martins, "Synthesis and characterization of magnetoliposomes for MRI contrast enhancement," *International Journal of Pharmaceutics*, vol. 446, no. 1–2, pp. 183–190, Mar. 2013, doi: 10.1016/j.ijpharm.2013.02.025.
[8] M. Morais *et al.*, "Radiolabeled Mannosylated Dextran Derivatives Bearing an NIR-Fluorophore for Sentinel Lymph Node Imaging," *Bioconjugate Chem.*, vol. 25, no. 11, pp. 1963–1970, Nov. 2014, doi: 10.1021/bc500336a.
[9] J. C. Matos, M. C. Gonçalves, L. C. Pereira, B. J. Vieira, and J. C. Waerenborgh, "SPIONs prepared in air through improved synthesis methodology: the influence of γ-Fe2O3/Fe3O4 ratio and coating composition on magnetic properties," *Nanomaterials*, vol. 9, no. 7, p. 943, 2019, doi: 10.3390/nano9070943.
[10] P. I. P. Soares *et al.*, "Effects of surfactants on the magnetic properties of iron oxide colloids," *Journal of Colloid and Interface Science*, vol. 419, pp. 46–51, Apr. 2014, doi: 10.1016/j.jcis.2013.12.045.
[11] A. S. Saraiva *et al.*, "3D-printed platform multi-loaded with bioactive, magnetic nanoparticles and an antibiotic for re-growing bone tissue," *International Journal of Pharmaceutics*, vol. 593, p. 120097, Jan. 2021, doi: 10.1016/j.ijpharm.2020.120097.
[12] C. Caro *et al.*, "Fe3O4-Au core-shell nanoparticles as a multimodal platform for in vivo imaging and focused photothermal therapy," *Pharmaceutics*, vol. 13, no. 3, Mar. 2021, doi: 10.3390/pharmaceutics13030416.
[13] N. S. Elbialy, M. M. Fathy, and W. M. Khalil, "Preparation and characterization of magnetic gold nanoparticles to be used as doxorubicin nanocarriers," *Physica Medica*, vol. 30, no. 7, pp. 843–848, Nov. 2014, doi: 10.1016/j.ejmp.2014.05.012.
[14] F. Silva *et al.*, "Interrogating the Role of Receptor-Mediated Mechanisms: Biological Fate of Peptide-Functionalized Radiolabeled Gold Nanoparticles in Tumor Mice," *Bioconjugate Chem.*, vol. 27, no. 4, pp. 1153–1164, Apr. 2016, doi: 10.1021/acs.bioconjchem.6b00102.
[15] G. J. Long, T. Cranshaw, and G. Longworth, "The ideal Mössbauer effect absorber thickness," *Mössbauer effect reference and data journal*, vol. 6, no. 2, pp. 42–49, 1983.
[16] J. Hesse and A. Rubartsch, "Model independent evaluation of overlapped Mossbauer spectra," *Journal of Physics E: Scientific Instruments*, vol. 7, no. 7, p. 526, 1974.
[17] S. Mahadevan, G. Gnanaprakash, J. Philip, B. P. C. Rao, and T. Jayakumar, "X-ray diffraction-based characterization of magnetite nanoparticles in presence of goethite and correlation with magnetic properties," *Physica E: Low-dimensional Systems and Nanostructures*, vol. 39, no. 1, pp. 20–25, Jul. 2007, doi: 10.1016/j.physe.2006.12.041.
[18] Hari-Bala *et al.*, "Controlling the particle size of nanocrystalline titania via a thermal dissociation of substrates with ammonium chloride," *Materials Letters*, vol. 60, no. 4, pp. 494–498, Feb. 2006, doi: 10.1016/j.matlet.2005.09.030.
[19] J. F. Dorsey *et al.*, "Gold nanoparticles in radiation research: potential applications for imaging and radiosensitization," *Translational Cancer Research*, vol. 2, no. 4, p. 12, 2013.
[20] S. Fatimah, R. Ragadhita, D. Fitria, A. Husaeni, A. Bayu, and D. Nandiyanto, "How to Calculate Crystallite Size from X-Ray Diffraction (XRD) using Scherrer Method," *ASEAN Journal of Science and Engineering*, pp. 65–76, 2021, doi: 10.17509/ijost.v6ix.
[21] I. Ostolska and M. Wiśniewska, "Application of the zeta potential measurements to explanation of colloidal Cr2O3 stability mechanism in the presence of the ionic polyamino acids," *Colloid Polym Sci*, vol. 292, no. 10, pp. 2453–2464, Oct. 2014, doi: 10.1007/s00396-014-3276-y.
[22] J. J. Carlson and S. K. Kawatra, "Factors Affecting Zeta Potential of Iron Oxides," *Mineral Processing and Extractive Metallurgy Review*, vol. 34, no. 5, pp. 269–303, Aug. 2013, doi: 10.1080/08827508.2011.604697.
[23] S. Honary and F. Zahir, "Effect of Zeta Potential on the Properties of Nano-Drug Delivery Systems - A Review (Part 1)," *Trop. J. Pharm Res*, vol. 12, no. 2, pp. 255–264, May 2013, doi: 10.4314/tjpr.v12i2.19.
[24] G. da Silva *et al.*, "Studies of the Colloidal Properties of Superparamagnetic Iron Oxide Nanoparticles Functionalized with Platinum Complexes in Aqueous and PBS Buffer Media," *J. Braz. Chem. Soc.*, 2016, doi: 10.21577/0103-5053.20160221.
[25] J. Stetefeld, S. A. McKenna, and T. R. Patel, "Dynamic light scattering: a practical guide and applications in biomedical sciences," *Biophys Rev*, vol. 8, no. 4, pp. 409–427, Dec. 2016, doi: 10.1007/s12551-016-0218-6.
[26] O. Karaagac, H. Kockar, S. Beyaz, and T. Tanrisever, "A Simple Way to Synthesize Superparamagnetic Iron Oxide Nanoparticles in Air Atmosphere: Iron Ion Concentration Effect," *IEEE Trans. Magn.*, vol. 46, no. 12, pp. 3978–3983, Dec. 2010, doi: 10.1109/TMAG.2010.2076824.
[27] L. Gholami, R. Kazemi Oskuee, M. Tafaghodi, A. Ramezani Farkhani, and M. Darroudi, "Green facile synthesis of low-toxic superparamagnetic iron oxide nanoparticles (SPIONs) and their cytotoxicity effects toward Neuro2A and HUVEC cell lines," *Ceramics International*, vol. 44, no. 8, pp. 9263–9268, Jun. 2018, doi: 10.1016/j.ceramint.2018.02.137.
[28] M. Barrow *et al.*, "Co-precipitation of DEAE-dextran coated SPIONs: how synthesis conditions affect particle properties, stem cell labelling and MR contrast," *Contrast media & molecular imaging*, vol. 11, no. 5, pp. 362–370, 2016.
[29] R. Stein *et al.*, "Synthesis and Characterization of Citrate-Stabilized Gold-Coated Superparamagnetic Iron Oxide Nanoparticles for Biomedical Applications," *Molecules*, vol. 25, no. 19, p. 4425, Sep. 2020, doi: 10.3390/molecules25194425.
[30] G. F. Goya, T. S. Berquó, F. C. Fonseca, and M. P. Morales, "Static and dynamic magnetic properties of spherical magnetite nanoparticles," *Journal of Applied Physics*, vol. 94, no. 5, pp. 3520–3528, Sep. 2003, doi: 10.1063/1.1599959.
[31] M. A. Gonzalez-Fernandez *et al.*, "Magnetic nanoparticles for power absorption: Optimizing size, shape and magnetic properties," *Journal of Solid State Chemistry*, vol. 182, no. 10, pp. 2779–2784, Oct. 2009, doi: 10.1016/j.jssc.2009.07.047.
[32] K. Mahmoudi, A. Bouras, D. Bozec, R. Ivkov, and C. Hadjipanayis, "Magnetic hyperthermia therapy for the treatment of glioblastoma: a review of the therapy's history, efficacy and application in humans," *International Journal of Hyperthermia*, vol. 34, no. 8, pp. 1316–1328, Nov. 2018, doi: 10.1080/02656736.2018.1430867.
[33] O. L. Lanier *et al.*, "Evaluation of magnetic nanoparticles for magnetic fluid hyperthermia," *International Journal of Hyperthermia*, vol. 36, no. 1, pp. 686–700, Jan. 2019, doi: 10.1080/02656736.2019.1628313.
[34] R. D. Piazza *et al.*, "PEGlatyon-SPION surface functionalization with folic acid for magnetic hyperthermia applications," *Mater. Res. Express*, vol. 7, no. 1, p. 015078, Jan. 2020, doi: 10.1088/2053-1591/ab6700.
[35] A. Szpak *et al.*, "T1–T2 Dual-modal MRI contrast agents based on superparamagnetic iron oxide nanoparticles with surface attached gadolinium complexes," *J Nanopart Res*, vol. 16, no. 11, p. 2678, Nov. 2014, doi: 10.1007/s11051-014-2678-6.
[36] A. Szpak, G. Kania, T. Skórka, W. Tokarz, S. Zapotoczny, and M. Nowakowska, "Stable aqueous dispersion of superparamagnetic iron oxide nanoparticles protected by charged chitosan derivatives," *J Nanopart Res*, vol. 15, no. 1, p. 1372, Jan. 2013, doi: 10.1007/s11051-012-1372-9.
[37] A. Sudame, G. Kandasamy, and D. Maity, "Single and Dual Surfactants Coated Hydrophilic Superparamagnetic Iron Oxide Nanoparticles for Magnetic Fluid Hyperthermia Applications," *j nanosci nanotechnol*, vol. 19, no. 7, pp. 3991–3999, Jul. 2019, doi: 10.1166/jnn.2019.16326.
[38] M. Di Marco, M. Port, P. Couvreur, C. Dubernet, P. Ballirano, and C. Sadun, "Structural Characterization of Ultrasmall Superparamagnetic Iron Oxide (USPIO) Particles in Aqueous Suspension by Energy Dispersive X-ray Diffraction (EDXD)," *J. Am. Chem. Soc.*, vol. 128, no. 31, pp. 10054–10059, Aug. 2006, doi: 10.1021/ja061674y.